therefore interpret the jump as the inclusion of at least one molecule in the gap between electrodes[20]. We stop the electromigration process once this happens, and study the devices at lower V.

The differential conductance $\partial I/\partial V$ for one such device is shown in Fig 4b. The most notable property is a peak in $\partial I/\partial V$ at $V = 0$. The peak has a logarithmic temperature dependence between 3 and 20 K (Fig. 4c). The peak also splits in an applied magnetic field (Fig. 4d), with a splitting equal to $2g\mu_B H$, where $g \approx 2$ and μ_B is the Bohr magneton. This peak has been clearly observed in about 30% of ~100 wires broken with the molecule, but is absent in clean gold electrodes, showing that it arises from the presence of the molecule.

The logarithmic temperature dependence and the magnetic-field splitting indicate that the peak is due to the Kondo effect[21]. The Kondo effect is the formation of a bound state between a local spin on an island and the conduction electrons in the electrodes that enhances the conductance at low biases. The observation of the Kondo effect is consistent with the identification of $S = 1/2$ for the Co^{2+} ion given above. By setting the low-temperature full-width at half-maximum of the Kondo peak equal to $2k_B T_K/e$, where T_K is the Kondo temperature[22,23], we estimate that T_K in different devices varies between 10 and 25 K. These large Kondo temperatures indicate that the coupling between the localized state and the island is strong, consistent with the high conductances found for the shorter linker molecule. In three devices the gate coupling was strong enough that T_K was increased by sweeping V_g to more negative values, indicating that the energy of the electronic state on the ion is tuned closer to the Fermi level. These devices thus provide an atomic-scale realization of the Kondo model, with Kondo temperatures higher than have been previously reported in quantum dots[24] or nanotubes[23].

We have made transistors from a single molecular complex in which one cobalt ion is connected to gold electrodes by organic barriers. By tuning the length of the organic barrier, we are able to control the coupling between the ion and the electrodes. For relatively long linker molecules, giving weak coupling, the molecule functions as a single-electron transistor. For stronger coupling, we observe Kondo-assisted tunnelling. We believe that the ability to design the electronic states of a molecular device using chemical techniques, together with the ability to measure individual molecules, will be important in molecular electronics and in the study of the physics of nanometre-scale systems. □

Methods

Synthesis of the molecules

The longer molecule investigated, $[Co(tpy\text{-}(CH_2)_5\text{-}SH)_2]^{2+}$, was synthesized from an ethanolic solution of 4′-(5-mercaptopentyl)-2,2′:6′,2″-terpyridinyl (tpy-$(CH_2)_5$-SH) and aqueous $CoCl_2$ (ref. 12). The shorter molecule, $[Co(tpy\text{-}SH)_2]^{2+}$, was a complex of cobalt with 4′-(mercapto)-2,2′:6′,2″-terpyridinyl (tpy-SH). The tpy-SH ligand was prepared from 4′-chloro-2,2′:6′,2″ terpyridinyl and sodium ethanethiolate by a nucleophilic aromatic substitution followed by nucleophilic aliphatic substitution to give the thiolate anion and subsequent protonation to give the desired compound[25,26].

Received 18 February; accepted 29 April 2002; doi:10.1038/nature00791.

1. Aviram, A. & Ratner, M. A. Molecular rectifiers. *Chem. Phys. Lett.* **29,** 277–283 (1974).
2. Chen, J., Reed, M. A., Rawlett, A. M. & Tour, J. M. Large on-off ratios and negative differential resistance in a molecular electronic device. *Science* **286,** 1550–1552 (1999).
3. Collier, C. P. *et al.* Electronically configurable molecular-based logic gates. *Science* **285,** 391–394 (1999).
4. Reed, M. A., Zhou, C., Muller, C. J., Burgin, T. P. & Tour, J. M. Conductance of a molecular junction. *Science* **278,** 252–254 (1997).
5. Kergueris, C. *et al.* Electron transport through a metal-molecule-metal junction. *Phys. Rev. B* **59,** 12505–12513 (1999).
6. Bumm, L. A. *et al.* Are single molecular wires conducting? *Science* **271,** 1705–1707 (1996).
7. Cui, X. D. *et al.* Reproducible measurement of single-molecule conductivity. *Science* **294,** 571–574 (2001).
8. Dekker, C. Carbon nanotubes as molecular quantum wires. *Phys. Today* **52,** 22–28 (1999).
9. Park, H. *et al.* Nanomechanical oscillations in a single-C_{60} transistor. *Nature* **407,** 57–60 (2000).
10. Schön, J. H., Meng, H. & Bao, Z. Field-effect modulation of the conductance of single molecules. *Science* **294,** 2138–2140 (2001).
11. Bard, A. J. & Faulkner, L. R. *Electrochemical Methods: Fundamentals and Applications* (Wiley & Sons, New York, 2001).
12. Maskus, M. & Abruna, H. D. Synthesis and characterization of redox-active metal complexes sequentially self-assembled onto gold electrodes via a new thiol-terpyridine ligand. *Langmuir* **12,** 4455–4462 (1996).
13. Park, H., Lim, A. K. L., Park, J., Alivisatos, A. P. & McEuen, P. L. Fabrication of metallic electrodes with nanometer separation by electromigration. *Appl. Phys. Lett.* **75,** 301–303 (1999).
14. Grabert, H. & Devoret, M. H. *Single Charge Tunneling: Coulomb Blockade Phenomena in Nanostructures* (Plenum, New York, 1992).
15. Deshmukh, M. M., Bonet, E., Pasupathy, A. N. & Ralph, D. C. Equilibrium and nonequilibrium electron tunneling via discrete quantum states. *Phys. Rev. B* **65,** 073301-1–073301-4 (2002).
16. Bonet, E., Deshmukh, M. M. & Ralph, D. C. Solving rate equations for electron tunneling via discrete quantum states. *Phys. Rev. B* **65,** 045317-1–045317-10 (2002).
17. Akera, H. Coulomb staircase and total spin in quantum dots. *Phys. Rev. B* **60,** 10683–10686 (1999).
18. Ralph, D. C., Black, C. T. & Tinkham, M. Gate-voltage studies of discrete electronic states in aluminum nanoparticles. *Phys. Rev. Lett.* **78,** 4087–4090 (1997).
19. Oshio, H., Spiering, H., Ksenofontov, V., Renz, F. & Guetlich, P. Electronic relaxation phenomena following $^{57}Co(EC)^{57}Fe$ nuclear decay in $[Mn^{II}(terpy)_2](ClO_4)_2.1/2H_2O$ and in the spin crossover complexes $[Co^{II}(terpy)_2]X_2.nH_2O$ (X = Cl and ClO_4): A Moessbauer emission spectroscopic study. *Inorg. Chem.* **40,** 1143–1150 (2001).
20. Bezryadin, A., Dekker, C. & Schmid, G. Electrostatic trapping of single conducting nanoparticles between nanoelectrodes. *Appl. Phys. Lett.* **71,** 1273–1275 (1999).
21. Wolf, E. L. *Principles of Electron Tunneling Spectroscopy* Ch. 8 (Oxford Univ. Press, Oxford, 1989).
22. van der Wiel, W. G. *et al.* The Kondo effect in the unitary limit. *Science* **289,** 2105–2108 (2000).
23. Nygård, J., Cobden, D. H. & Lindelof, P. E. Kondo physics in carbon nanotubes. *Nature* **408,** 342–346 (2000).
24. Goldhaber-Gordon, D. *et al.* Kondo effect in a single-electron transistor. *Nature* **391,** 156–159 (1998).
25. Testaferri, L., Tiecco, M., Tingoli, M., Chianelli, D. & Montanucci, M. Simple syntheses of aryl alkyl thioethers and of aromatic thiols from unactivated aryl halides and efficient methods for selective dealkylation of aryl alkyl ethers and thioethers. *Synthesis (Stuttgart)* **9,** 751–755 (1983).
26. Mathis, J. M. & Pallenberg, A. J. Preparation of novel, functionalized 1,10-phenanthrolines. *Synth. Commun.* **27,** 2943–2951 (1997).

Acknowledgements

We thank E. Smith, M. Brink and J.-Y. Park for help with measurements, and M. Deshmukh for discussions. This work was supported by NSF, through individual-investigator grants, the Cornell Center for Materials Research, and the use of the National Nanofabrication Users Network. Support was also provided by the Packard Foundation, the US Department of Energy and Department of Education GAANN fellowships.

Competing interests statement

The authors declare that they have no competing financial interests.

Correspondence and requests for materials should be addressed to P.M. (e-mail: mceuen@ccmr.cornell.edu) or D.R. (e-mail: ralph@ccmr.cornell.edu).

Kondo resonance in a single-molecule transistor

Wenjie Liang*, Matthew P. Shores†, Marc Bockrath*, Jeffrey R. Long† & Hongkun Park*

** Department of Chemistry and Chemical Biology, Harvard University, 12 Oxford Street, Cambridge, Massachusetts 02138, USA*
† Department of Chemistry, University of California, Berkeley, California 94720, USA

When an individual molecule[1], nanocrystal[2–4], nanotube[5,6] or lithographically defined quantum dot[7] is attached to metallic electrodes via tunnel barriers, electron transport is dominated by single-electron charging and energy-level quantization[8]. As the coupling to the electrodes increases, higher-order tunnelling and correlated electron motion give rise to new phenomena[9–19], including the Kondo resonance[10–16]. To date, all of the studies of Kondo phenomena in quantum dots have been performed on systems where precise control over the spin degrees of freedom is difficult. Molecules incorporating transition-metal atoms provide powerful new systems in this regard, because the spin and orbital degrees of freedom can be controlled through well-defined chemistry[20,21]. Here we report the observation of the Kondo effect in single-molecule transistors, where an individual divanadium molecule[20] serves as a spin impurity. We find that the

Kondo resonance can be tuned reversibly using the gate voltage to alter the charge and spin state of the molecule. The resonance persists at temperatures up to 30 K and when the energy separation between the molecular state and the Fermi level of the metal exceeds 100 meV.

We prepared devices by an extension of the methods previously used in constructing single-C_{60} (ref. 1) and single-nanocrystal transistors[3]. Using electron-beam lithography, a narrow gold bridge was fabricated on an aluminium pad with a ~3-nm oxide layer serving as a gate electrode[22]. The electromigration-induced break-junction technique[1,3] was then used to create two closely spaced gold electrodes (Fig. 1). Scanning electron microscope imaging and tunnel current measurements reveal that the narrowest gap between the two electrodes is consistently ~1 nm.

Single-molecule transistors containing individual divanadium (V_2) molecules ([(*N*,*N*′,*N*″-trimethyl-1,4,7-triazacyclononane)$_2$-$V_2(CN)_4(\mu\text{-}C_4N_4)$]: Fig. 1)[20] were prepared by depositing a dilute methanol solution of the V_2 molecule onto the gold bridge. To minimize the probability of multiple V_2 molecules bridging two electrodes, we controlled the coverage of molecules on an array of gold electrodes such that <20% of the junctions—7 in an array of 42 broken junctions—showed current–voltage (*I*–*V*) characteristics different from a simple tunnel junction.

Figure 2 shows plots of differential conductance ($\partial I/\partial V$) as a function of bias voltage (V) and gate voltage (V_g) for two single-V_2 transistors, designated D1 and D2. Two distinct characteristics, which are shared by all seven single-V_2 transistors studied to date, are evident in the behaviour of both devices. Each displays two conductance-gap regions, I and II, bounded by two broad $\partial I/\partial V$ peaks that slope linearly as a function of V_g. These peaks cross at $V_g = V_c$, at which point the conductance gaps vanish. Moving away from this point, the gaps in both regions continue to widen even beyond $V = 100$ mV. Most significantly, the devices also exhibit a sharp zero-bias $\partial I/\partial V$ peak in region I, whereas this peak is clearly absent in region II. The zero-bias $\partial I/\partial V$ peak was generally found to persist up to $T \geq 10$ K. Other features observable in D2, such as the enhanced conductance within region I and the $\partial I/\partial V$ peaks outside the conductance gaps, were not shared by all devices (see below).

The observation of conductance gaps that vary linearly with V_g provides strong experimental evidence that an individual molecule is responsible for the device behaviour. A conductance gap arises from the finite energy required to add (remove) an electron to (from) the molecule, which is a consequence of single-electron charging and the quantized molecular level spacing. The conductance gap changes linearly and reversibly as a function of V_g because a more positive V_g stabilizes an additional electron on the V_2 molecule. At the charge degeneracy point, $V_g = V_c$, where the total energy is the same for two different charge states of the molecule, the conductance gap disappears. As V_g traverses V_c in the positive direction, the equilibrium number of charges on the molecule increases by one electron.

Certainly the most prominent feature of the data is the appear-

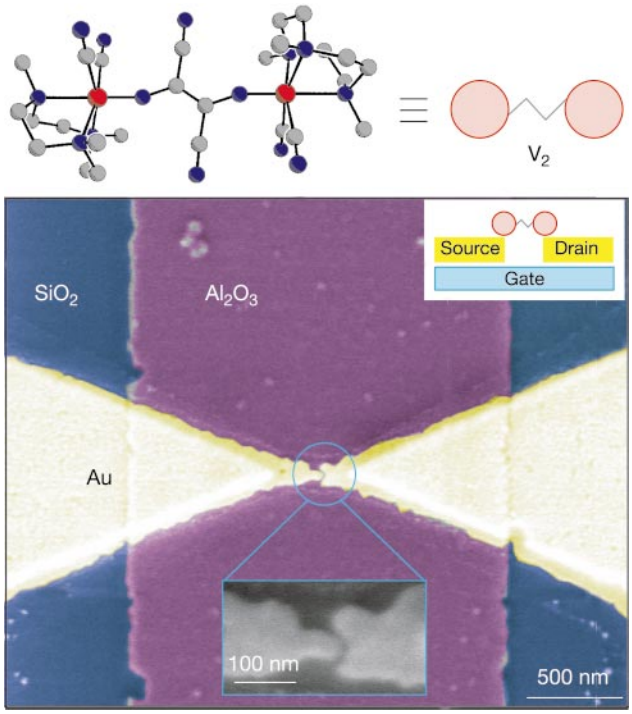

Figure 1 Fabrication of single-molecule transistors incorporating individual divanadium molecules. Top left, the structure of [(*N*,*N*′,*N*″-trimethyl-1,4,7-triazacyclononane)$_2$$V_2(CN)_4(\mu\text{-}C_4N_4)$] (the V_2 molecule) as determined by X-ray crystallography; red, grey and blue spheres represent respectively V, C and N atoms. Top right, the schematic representation of this molecule. Main panel, scanning electron microscope image (false colour) of the metallic electrodes fabricated by electron beam lithography and the electromigration-induced break-junction technique. The image shows two gold electrodes separated by ~1 nm above an aluminium pad, which is covered with an ~3-nm-thick layer of aluminium oxide. The whole structure was defined on a silicon wafer. The bright yellow regions correspond to a gold bridge with a thickness of 15 nm and a minimum lateral size of ~100 nm. The paler yellow regions represent portions of the gold electrodes with a thickness of ~100 nm. Main panel inset, schematic diagram of a single-V_2 transistor.

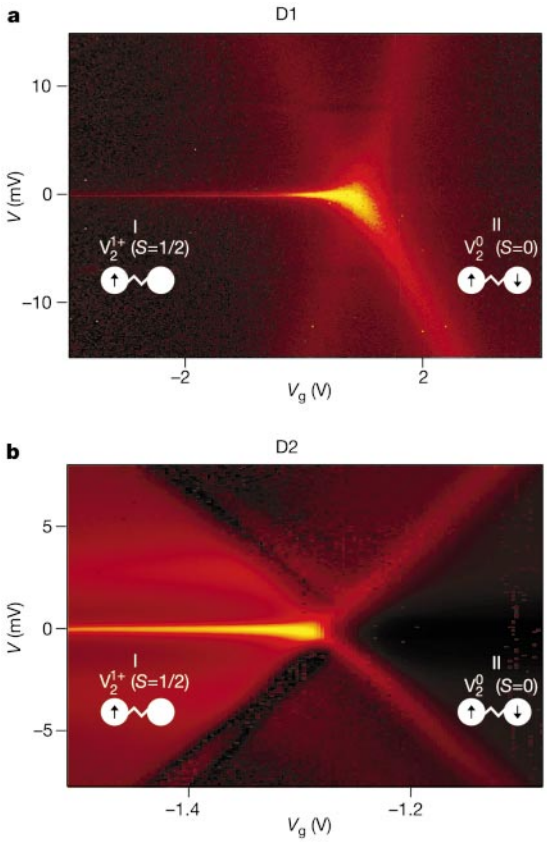

Figure 2 Plots of differential conductance ($\partial I/\partial V$) as a function of bias voltage (V) and gate voltage (V_g) obtained from two different single-V_2 transistors D1 (**a**) and D2 (**b**). Both measurements were performed at $T = 300$ mK. The $\partial I/\partial V$ values are represented by the colour scale, which changes in **a**, from dark red (0) to bright yellow ($1.55e^2/h$) and in **b**, from dark red (0) to bright yellow ($1.3\,e^2/h$). The value of e^2/h is 38.8 μS or $(25.8\,\text{k}\Omega)^{-1}$. The labels I and II mark two conductance-gap regions, and the diagrams indicate the charge and spin states of the V_2 molecule in each region.

ance of the sharp zero-bias $\partial I/\partial V$ peak in region I. This feature is strongly reminiscent of the Kondo resonance observed previously in lithographically defined quantum dots[10–14] and single-walled carbon nanotubes[15,16]. The Kondo resonance is a many-electron phenomenon resulting from the exchange interaction between a localized spin and the conduction electrons in metallic electrodes[17–19,23,24], and it appears only when the electronic state of a quantum dot has non-zero spin (S) or degeneracy.

One signature of a Kondo resonance arising from non-zero S is the splitting of its peak position in an applied magnetic field, B, by twice the ordinary Zeeman splitting[19]. Figure 3a depicts a plot of $\partial I/\partial V$ versus V and B, and clearly shows that the zero-bias $\partial I/\partial V$ peak in region I splits in V under a magnetic field. The magnitude of this splitting is 230 μV T^{-1} or $2g\mu_B B/e$ (where $g = 2$ is the g-factor of the molecule[20], and μ_B is the Bohr magneton), consistent with the expected splitting of a Kondo resonance. As the temperature is raised, the peak height of the resonance is expected to decrease in a characteristic fashion while its peak width increases (see below for further discussion)[12,17,24]. Such behaviour is evident in the data presented in Fig. 4. These observations therefore firmly establish that the zero-bias $\partial I/\partial V$ peaks in region I arise from a Kondo resonance in the single-V_2 transistors.

The absence of a Kondo resonance in region II suggests, on the other hand, that the requisite spin degeneracy is lost when the charge state of the V_2 molecule changes by the addition of one electron. Insight into the origin of this behaviour can be obtained by inspecting Fig. 3b, which displays a $\partial I/\partial V$–V–V_g plot analogous to those in Fig. 2, but with data measured at $B = 8$ T. In particular, Fig. 3b shows that the $\partial I/\partial V$ peaks defining region II exhibit an ordinary Zeeman splitting of $g\mu_B B/e = 115\,\mu$V T^{-1}, whereas the peaks defining region I show no such splitting. This splitting pattern is characteristic of the ground-state spin change of $\Delta S = -1/2$ upon the addition of one electron[25]. Comparison of Figs 2b and 3b further shows that the charge degeneracy point ($V_g = V_c$) moves in the positive V_g direction as the magnetic field is increased, signifying that the ground state of the molecule in region I is stabilized relative to that in region II. Analysis of this shift on the basis of the known electrostatic coupling to the gate electrode indicates that the energy stabilization amounts to $\sim$100 μV T^{-1}, again consistent with a reduction of the spin by 1/2.

In the neutral V_2 molecule, both vanadium atoms exist in a 4+ oxidation state, each possessing one valence d electron[20] (Fig. 3c). Electrochemical studies show that in organic solvents three oxidation states of the V_2 molecule are accessible[20]: neutral V_2^0, positive V_2^+, and negative V_2^-. Magnetic measurements performed on bulk samples indicate that the ground state of V_2^0 is a spin-singlet ($S = 0$) owing to the antiferromagnetic coupling between vanadium centres, while that of V_2^- is a spin-quadruplet ($S = 3/2$) owing to the resonant exchange of the added electron[20]. Although the V_2^+ ion has not yet been isolated in bulk, the ground state of V_2^+ is expected to be a spin-doublet ($S = 1/2$) as it possesses only one d electron. These results, combined with the information that the ground-state spin value reduces by 1/2 upon one-electron addition, indicate that the V_2^+ and V_2^0 species are responsible for the device behaviour in regions I and II, respectively, as shown in Fig. 2.

Determination of the spin multiplicity permits a quantitative analysis of the temperature dependence of the Kondo effect (Fig. 4). Previous theoretical[17–19,23,24] and experimental[10–16] studies have shown that the Kondo physics of a non-degenerate spin-1/2 system is characterized by a single temperature scale known as the Kondo temperature (T_K). In the limit of a large charging energy U ($U > 1$ eV in the V_2 molecule) and $\varepsilon \gg \Gamma$, T_K is expected to follow the functional form[7,26] $T_K = 0.5(\Gamma U)^{1/2}\exp(-\pi\varepsilon/\Gamma)$. Here Γ is the level width due to the tunnel coupling to metallic electrodes, and $-\varepsilon$ is the energy of the localized electron measured relative to the metal Fermi level. Although this expression is derived in the Kondo regime ($\varepsilon/\Gamma \gg 1$), previous experimental studies have shown that the expression also adequately describes data in the crossover region between the mixed-valence ($\varepsilon/\Gamma \leq 0.5$) and the Kondo regimes[12,14]. The temperature dependence of the Kondo peak height (G_K) follows an approximate scaling form given by $G_K(T) = G_0/(1 + (2^{1/s} - 1)T^2/T_K^2)^s$, where G_0 is a constant[12]. The value of s depends on the value of ε/Γ, and it attains its asymptotic value of 0.22 when $\varepsilon/\Gamma \gg 1$. At low temperatures, the width of the Kondo peak is expected to saturate at $\sim k_B T_K/e$, where k_B is the Boltzmann constant[11].

T_K and the resonance width extracted from device D3 are presented as a function of ε/Γ in Fig. 4b. The value of T_K was determined by fitting the measured G_K–T curves to the above scaling expression using G_0 and s as fit parameters, and the peak width was measured at the full-width at half-maximum. We note that the T_K value close to $V_g = V_c$ exceeds 30 K, representing (to our knowledge) the highest Kondo temperature reported to date for a quantum-dot type system. Far away from $V_g = V_c$, the peak widths converge to an asymptotic value owing to thermal broadening. The Kondo resonance nevertheless persists even when ε exceeds 100 meV ($\varepsilon/\Gamma > 3$).

Figure 4b shows that, as ε is tuned away from the Fermi level, both T_K and the peak width decay as expected, but they do not follow a single-exponential form. The values of ε/Γ range from 0.1 to 2, thus spanning the mixed-valence regime ($\varepsilon/\Gamma \leq 0.5$) and crossing over to the Kondo regime ($\varepsilon/\Gamma \gg 1$) (refs 12, 24, 26, 27). As shown by two lines in Fig. 4b, the decay can be approximated by $\exp(-3\varepsilon/\Gamma)$ for $0 < \varepsilon/\Gamma < 0.5$ and then rolls over to $\exp(-1.3\varepsilon/\Gamma)$

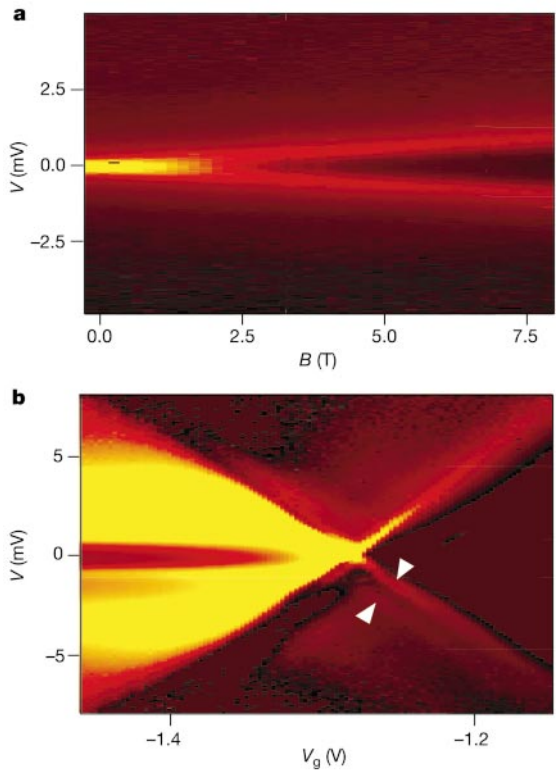

Figure 3 Transport data obtained from single-V_2 transistors in an applied magnetic field (B). **a**, A $\partial I/\partial V$ plot as a function of V and B obtained from D1 at $V_g = -0.1$ V and at $T = 300$ mK. The $\partial I/\partial V$ values are represented by a colour scale that varies from dark red (0) to bright yellow (1.3 e^2/h). **b**, A $\partial I/\partial V$ plot as a function of V and V_g obtained from D2 at $B = 8$ T and at $T = 300$ mK. White arrows indicate the two $\partial I/\partial V$ peaks that arise from a Zeeman splitting. To clearly illustrate weak Zeeman-split features, the colour scale has been changed from that in Fig. 2a and varies from dark red (0) to bright yellow (0.55 e^2/h).

for $0.5 < \varepsilon/\Gamma < 2$. In the range of $0.5 < \varepsilon/\Gamma < 2$, the decay is approximately a factor of two slower than what has been observed previously for a non-degenerate spin-1/2 system[12,14].

One possible explanation for this behaviour is that not only the spin but also orbital degrees of freedom may be required to explain the Kondo physics observed in single-V_2 transistors. As discussed previously, the V_2^+ ion contains two equivalent vanadium sites and hence it can provide doubly degenerate orbitals for a single d electron. Such degeneracy is known to be important from studies of lanthanide impurities in metal hosts[23,28,29], and theoretical calculations predict that the Kondo temperature scales as $T_K \propto \exp(-\pi\varepsilon/2\Gamma)$ for doubly degenerate orbital cases[23,28,29], therefore accounting for our experimental data in a satisfactory fashion. Nevertheless, given the experimental and theoretical uncertainties, this conclusion remains speculative, and further investigation is necessary to resolve the role of orbital degeneracy in the single-V_2-transistor system.

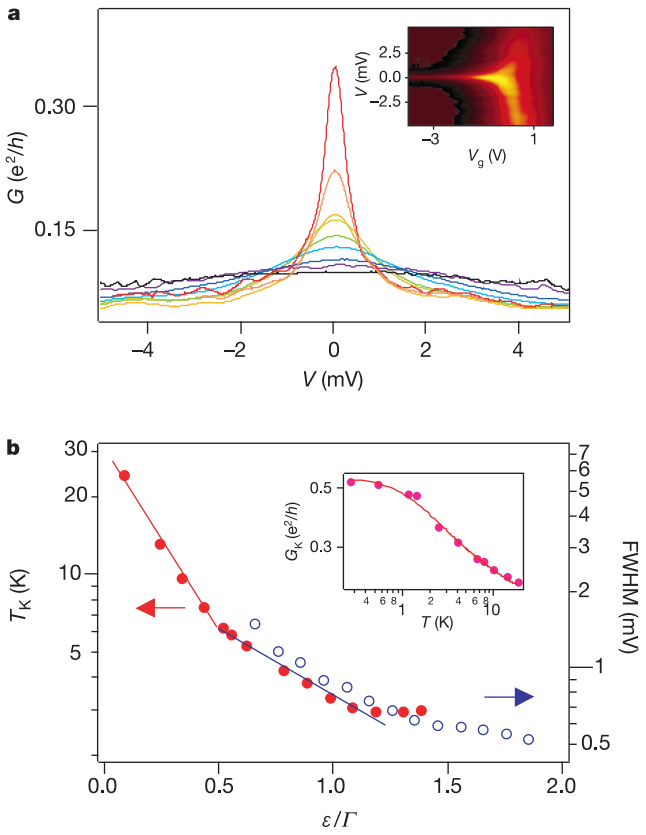

Figure 4 Temperature-dependent transport data from device D3. **a**, A plot of conductance (G) versus V with $V_g = -2.25$ V at various temperatures. The temperatures of the measurements (in K) are $T = 0.3$, 1.0, 2.0, 3.1, 4.2, 6.3, 9.0, 14 and 20, in order of decreasing peak height. Inset, a $\partial I/\partial V$ plot as a function of V and V_g at $T = 300$ mK. The colour scale changes from dark red (0) to bright yellow (0.55 e^2/h). **b**, The Kondo temperature (T_K: filled red circles) and the Kondo peak width determined by the full-width at half-maximum (open blue circles) plotted against ε/Γ in a logarithmic scale. Here $-\varepsilon$ is the energy of the localized electron measured relative to the Fermi level of the metal, and Γ is the level width due to the tunnel coupling to the metallic electrodes. Measurements of the $\partial I/\partial V$ peak widths and slopes that define conductance gaps (inset in **a**) show that Γ is ~30 mV and the gate coupling is $\alpha = C_g/C_\Sigma = 30\,\text{meV}\,V_g^{-1}$ (C_g is the capacitance to the gate, and C_Σ is the total capacitance). This value of α allows the conversion of V_g to ε, because $\varepsilon = \alpha(V_c - V_g)$. We estimate that the values of Γ and ε are accurate to within 20%. Red and blue lines are proportional to $\exp(-3\varepsilon/\Gamma)$ and $\exp(-1.3\varepsilon/\Gamma)$, respectively. As ε/Γ exceeds 2, T_K and the peak widths approach respective asymptotic values. Inset, plot of the Kondo peak height (G_K) as a function of temperature at $\varepsilon = 0.43\Gamma$. The line is a fit to the formula $G_K(T) = G_0/(1 + (2^{1/s} - 1)T^2/T_K^2)^s$, yielding $T_K = 12.2$ K and $s = 0.19$.

Overall, the behaviour of a single-V_2 transistor is well described by the Coulomb blockade model and a Kondo resonance originating from the V_2^+ ion. However, certain transport characteristics of these transistors remain to be explained. As noted previously, device D2 exhibits strongly enhanced conductance values within the nominal conductance-gap region I. The bias position of this feature does not depend on V_g, suggesting that it arises from inelastic cotunnelling events[16,30]. In addition, some devices exhibit one or more $\partial I/\partial V$ peaks outside the conductance gaps. Both observations suggest that the excited electronic or vibrational states may participate in electron transport[1].

The present study shows that molecules can provide a Kondo system where critical parameters of Kondo physics, such as the spin and orbital degrees of freedom, are defined by chemical synthesis. With the recent advances of synthetic methodology, the preparation of molecular clusters possessing adjustable magnetic properties is becoming feasible[21]. Future investigations of such species are expected to provide detailed insight into electron transport through a molecular system where the spin and orbital degeneracies are precisely controlled. □

Received 18 February; accepted 29 April 2002; doi:10.1038/nature00790.

1. Park, H. *et al.* Nano-mechanical oscillations in a single-C_{60} transistor. *Nature* **407,** 57–60 (2000).
2. Klein, D. L. *et al.* A single-electron transistor made from a cadmium selenide nanocrystal. *Nature* **389,** 699–701 (1997).
3. Park, H. *et al.* Fabrication of metallic electrodes with nanometer separation by electromigration. *Appl. Phys. Lett.* **75,** 301–303 (1999).
4. Banin, U., Cao, Y., Katz, D. & Millo, O. Identification of atomic-like electronic states in indium arsenide nanocrystal quantum dots. *Nature* **400,** 542–544 (1999).
5. Tans, S. J. *et al.* Individual single-wall carbon nanotubes as quantum wires. *Nature* **386,** 474–476 (1997).
6. Bockrath, M. *et al.* Single-electron transport in ropes of carbon nanotubes. *Science* **275,** 1922–1925 (1997).
7. Kouwenhoven, L. P. *et al.* Excitation spectra of circular few-electron quantum dots. *Science* **278,** 1788–1792 (1997).
8. Grabert, H. & Devoret, M. H. *Single Charge Tunneling* (Plenum, New York, 1992).
9. Liang, W. *et al.* Fabry-Perot interference in a nanotube electron waveguide. *Nature* **411,** 665–669 (2001).
10. Goldhaber-Gordon, D. *et al.* Kondo effect in a single-electron transistor. *Nature* **391,** 156–159 (1998).
11. Cronenwett, S. M., Oosterkamp, T. H. & Kouwenhoven, L. P. A tunable Kondo effect in quantum dots. *Science* **281,** 540–544 (1998).
12. Goldhaber-Gordon, D. *et al.* From the Kondo regime to the mixed-valence regime in a single-electron transistor. *Phys. Rev. Lett.* **81,** 5225–5228 (1998).
13. Schmid, J., Weis, J., Eberl, K. & Klitzing, K. v. Absence of odd-even parity behaviour for Kondo resonances in quantum dots. *Phys. Rev. Lett.* **84,** 5824–5827 (2000).
14. van der Wiel, W. G. *et al.* The Kondo effect in the unitary limit. *Science* **289,** 2105–2108 (2000).
15. Nygard, J., Cobden, D. H. & Lindelof, P. E. Kondo physics in carbon nanotubes. *Nature* **408,** 342–346 (2000).
16. Liang, W., Bockrath, M. & Park, H. Shell filling and exchange coupling in metallic single-walled carbon nanotubes. *Phys. Rev. Lett.* **88,** 126801-1–126801-4 (2002).
17. Glazman, L. I. & Raikh, M. E. Resonant Kondo transparency of a barrier with quasilocal impurity states. *JETP Lett.* **47,** 452–455 (1988).
18. Ng, T. K. & Lee, P. A. On-site Coulomb repulsion and resonant tunneling. *Phys. Rev. Lett.* **61,** 1768–1771 (1988).
19. Meir, Y., Wingreen, N. S. & Lee, P. A. Low-temperature transport through a quantum dot: The Anderson model out of equilibrium. *Phys. Rev. Lett.* **70,** 2601–2604 (1993).
20. Shores, M. P. & Long, J. R. Tetracyanide-bridged divanadium complexes: Redox switching between strong antiferromagnetic and strong ferromagnetic coupling. *J. Am. Chem. Soc.* **124,** 3512–3513 (2002).
21. Shores, M. P., Sokol, J. J. & Long, J. R. Nickel(II)-molybdenum(III)-cyanide clusters: Synthesis and magnetic behaviour of species incorporating $[(Me_3tacn\}Mo(CN)_3]$. *J. Am. Chem. Soc.* **124,** 2279–2292 (2002).
22. Bachtold, A., Hadley, P., Nakanishi, T. & Dekker, C. Logic circuits with carbon nanotube transistors. *Science* **294,** 1317–1320 (2001).
23. Schlottmann, P. Some exact results for dilute mixed-valent and heavy-fermion systems. *Phys. Rep.* **181,** 1–119 (1989).
24. Hewson, A. C. *The Kondo Problem to Heavy Fermions* (Cambridge Univ. Press, Cambridge, 1993).
25. Cobden, D. H. *et al.* Spin splitting and even-odd effects in carbon nanotubes. *Phys. Rev. Lett.* **81,** 681–684 (1998).
26. Haldane, F. D. M. Scaling theory of the asymmetric Anderson model. *Phys. Rev. Lett.*, 416–419 (1978).
27. Wingreen, N. S. & Meir, Y. Anderson model out of equilibrium: Noncrossing-approximation approach to transport through a quantum dot. *Phys. Rev. B* **49,** 11040–11052 (1994).
28. Lin, H. Q. & Hirsch, J. E. Magnetic properties of a degenerate Anderson impurity. *Phys. Rev. B* **37,** 1864–1873 (1988).
29. Bonca, J. & Gubernatis, J. E. Quantum Monte Carlo simulations of the degenerate single-impurity Anderson model. *Phys. Rev. B* **47,** 13137–13146 (1993).
30. De Franceschi, S. *et al.* Electron cotunneling in a semiconductor quantum dot. *Phys. Rev. Lett.* **86,** 878–881 (2001).

Acknowledgements

We thank C. Lieber, B. Halperin and D. R. Reichman for discussions. This work was supported by NSF, DARPA, the Dreyfus Foundation, the Packard Foundation, the Research Corporation, and Harvard University (H.P.) and NSF (J.R.L.). M.B. is partially supported by the Department of Physics, Harvard University.

Competing interests statement

The authors declare that they have no competing financial interests.

Correspondence and requests for materials should be addressed to H.P. (e-mail: HPark@chemistry.harvard.edu).

Mycorrhizal weathering of apatite as an important calcium source in base-poor forest ecosystems

Joel D. Blum*, Andrea Klaue*, Carmen A. Nezat*, Charles T. Driscoll†, Chris E. Johnson†, Thomas G. Siccama‡, Christopher Eagar§, Timothy J. Fahey‖ & Gene E. Likens¶

** Department of Geological Sciences, University of Michigan, 425 East University Avenue, Ann Arbor, Michigan 48109, USA*
† Department of Civil and Environmental Engineering, Syracuse University, New York 13244, USA
‡ Yale School of Forestry and Environmental Studies, New Haven, Connecticut 06511, USA
§ Northeastern Research Station, USDA Forest Service, Durham, New Hampshire 03824, USA
‖ Department of Natural Resources, Cornell University, Ithaca, New York 14853, USA
¶ Institute of Ecosystem Studies, Millbrook, New York 12545, USA

The depletion of calcium in forest ecosystems of the northeastern USA[1–3] is thought to be a consequence of acidic deposition and to be at present restricting the recovery of forest and aquatic systems[4–7] now that acidic deposition itself is declining. This depletion of calcium has been inferred from studies[1–3] showing that sources of calcium in forest ecosystems—namely, atmospheric deposition and mineral weathering of silicate rocks such as plagioclase, a calcium-sodium silicate—do not match calcium outputs observed in forest streams. It is therefore thought that calcium is being lost from exchangeable and organically bound calcium in forest soils. Here we investigate the sources of calcium in the Hubbard Brook experimental forest, through analysis of calcium and strontium abundances and strontium isotope ratios within various soil, vegetation and hydrological pools. We show that the dissolution of apatite (calcium phosphate) represents a source of calcium that is comparable in size to known inputs from atmospheric sources and silicate weathering. Moreover, apatite-derived calcium was utilized largely by ectomycorrhizal tree species, suggesting that mycorrhizae may weather apatite and absorb the released ions directly, without the ions entering the exchangeable soil pool. Therefore, it seems that apatite weathering can compensate for some of the calcium lost from base-poor ecosystems, and should be considered when estimating soil acidification impacts and calcium cycling.

We studied the biogeochemistry of calcium in a mixed conifer/hardwood forest within a 12-ha watershed (W-1) at the Hubbard Brook experimental forest (HBEF), New Hampshire, USA[2,7,8]. The main calcium-bearing minerals present in soil parent material are plagioclase, K-feldspar, hornblende, pyroxene and apatite. Sequential digestions of soil samples (see Methods) were used to give information on the weathering sources of Ca (Table 1). We first examined the molar ratios of P/Ca versus Na/Ca in C-horizon digestions in comparison with the average composition of the main Ca-bearing minerals (Fig. 1). 'Digest 1' consisted mainly of dissolved apatite, consistent with the much faster ($>10^3$ times) dissolution rate of apatite compared to hornblende, plagioclase and K-feldspar (at pH 2–5)[9–11]. 'Digest 2' consisted mainly of dissolved hornblende and pyroxene (Fig. 1), and 'digest 3' was mainly dissolved plagioclase and K-feldspar. About 12% of the Ca in the soil parent material occurs in apatite, another 12% is in hornblende and pyroxene, and 76% is in feldspars. The Ca/Sr ratio of digest 1 was very different to that of digests 2 and 3 (Table 1), owing to differences in Sr substitution for Ca in silicate versus phosphate minerals—providing a tracer of apatite-derived Ca. The Ca/Sr ratio of digest 1 for each soil horizon suggests that apatite was depleted from the Oa, E, Bh and Bs1 horizons, but is present in the Bs2 and C horizons (Fig. 2). If we assume that all of the Ca in the C-horizon digest 1 is derived from apatite (Fig. 1), then a Ca/Sr mixing calculation[12,13] shows that 86% of the Ca released from the Bs2-horizon soils by digest 1 is derived from apatite.

We used Ca/Sr and $^{87}Sr/^{86}Sr$ ratios to ascertain the original sources of Ca in ecosystem pools[13–17]. The $^{87}Sr/^{86}Sr$ ratio is not changed by ion exchange, plant uptake or transport[13–19], and the Ca/Sr ratio has generally been observed to be only slightly changed by these processes (a factor of 1.0–1.6)[14,18,19]. The C-horizon digest-1 fractions had average Ca/Sr and $^{87}Sr/^{86}Sr$ ratios (respectively 2,580 and 0.72164) that were distinct from the values for the digest-2 (279 and 0.73669) and digest-3 fractions (170 and 0.73352; Fig. 3). This pattern is consistent with our interpretation that digest 1 is dominated by dissolution of apatite, which has characteristically

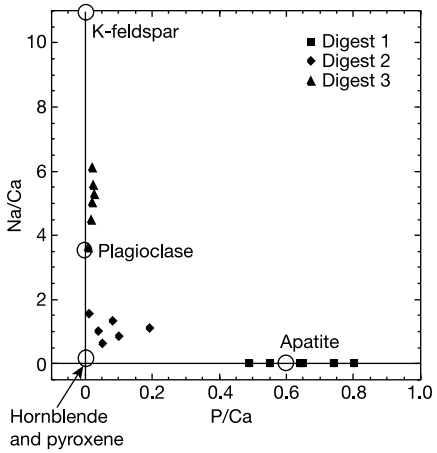

Figure 1 Major-element ratios of sequential digests of six composite C-horizon soil samples and soil minerals. See Methods for details.

Table 1 Average exchangeable and sequential digest concentrations

	Ca	K	Mg	Na	Si	P	Ca/Sr*
	μmol per g soil						
Exchangeable	0.01	0.50	<0.04	<0.04	0.09	0.02	281
Digest 1	24.0	1.45	6.21	0.27	36.9	16.0	2580
Digest 2	24.0	58.1	65.6	25.5	305	1.63	279
Digest 3	151	580	34.7	733	13200	3.04	170
Total soil (sum)	199	640	107	759	13500	20.7	202
	Percentage of total soil						
Exchangeable	0.05	0.08	<0.04	<0.01	<0.01	0.11	
Digest 1	12.0	0.23	5.83	0.04	0.27	77.3	
Digest 2	12.0	9.07	61.6	3.36	2.25	7.90	
Digest 3	75.9	90.6	32.5	96.6	97.5	14.7	

Data are shown for six composite C-horizon samples.
*Mole ratio.